coatings

MDPI

Article

Corrosion Resistance and Deuterium Aging Performance of α-Al_2O_3 Composite Hydrogen Permeation Barrier Coatings

Huayu Yang [1], Shiquan Liu [1], Xinyun Wang [1] and Heping Li [1,2,*]

[1] State Key Laboratory of Materials Processing and Die & Mould Technology, School of Materials Science and Engineering, Huazhong University of Science and Technology, Wuhan 430074, China
[2] Shenzhen Huazhong University of Science and Technology Research Institute, Shenzhen 518057, China
* Correspondence: liheping@hust.edu.cn

Abstract

Hydrogen permeation barriers (HPBs) are essential to the development of both hydrogen and nuclear fusion energy. However, their structural stability and barrier efficiency under extreme conditions are scarcely reported, despite their significant importance to practical applications. Here, we experimentally investigated the effect of Li_4SiO_4 corrosion and deuterium aging on the structure and performance of an α-Al_2O_3 composite hydrogen permeation barrier coating under simulated fusion conditions. The results demonstrate that this coating could retain its dense and defect-free structure after corrosion with Li_4SiO_4 powders at 550 °C for 2 days, exhibiting good tritium breeder compatibility. Moreover, after the deuterium aging test for 6 months, its phase composition and microstructure show no significant changes, maintaining a compact and crack-free matrix strongly bonded to the substrate. After 6-month aging, the hydrogen permeation resistance of the α-Al_2O_3 composite coating at 500 °C is still 1450 times higher than that of the steel substrate without any aging. This work provides critical insights into designing highly reliable hydrogen permeation barrier coatings and understanding their performance evolution under harsh fusion environments.

Keywords: hydrogen permeation barrier; Al_2O_3 coating; tritium breeder; Li_4SiO_4 corrosion; deuterium aging

1. Introduction

With the intensification of the global energy crisis and environmental degradation, developing clean, efficient, and sustainable alternative energy sources has become a paramount global research focus [1,2]. Controlled nuclear fusion is widely considered one of the most promising future energy options owing to its abundant fuel reserves, exceptionally high energy density, and environmental friendliness [3,4]. However, during the operation of fusion reactors, hydrogen isotopes such as deuterium (D) and tritium (T) readily permeate through structural materials under elevated temperatures, leading to severe issues including fuel loss, material hydrogen embrittlement, and radioactive contamination [5–7]. Currently, fabricating hydrogen permeation barrier coatings (HBCs) on the surfaces of tritium-handling components is recognized as one of the most effective strategies to suppress hydrogen isotope permeation [8].

Nevertheless, these HBCs confront highly complex environmental challenges during actual service, particularly corrosion induced by tritium breeders. Although lithium-bearing solid tritium breeders, such as Li_4SiO_4, exhibit desirable high-temperature stability

Check for updates

Academic Editor: Tadeusz Hryniewicz

Received: 2 July 2026
Revised: 1 August 2026
Accepted: 14 August 2026
Published: 17 August 2026

Copyright: © 2026 by the authors. Licensee MDPI, Basel, Switzerland. This article is an open access article distributed under the terms and conditions of the Creative Commons Attribution (CC BY) license.

and tritium release performance, the liberated or migrated lithium elements tend to diffuse into the HBCs and trigger chemical reactions. This interaction subsequently results in structural degradation and a concomitant decline in permeation resistance. Consequently, an ideal HBC must not only possess excellent deuterium/tritium barrier capabilities but also exhibit robust chemical corrosion resistance against tritium breeder environments.

Furthermore, exposure to a deuterium/tritium-rich environment is inevitable during the long-term operation of fusion reactors [9,10]. Due to their small atomic radii, hydrogen isotopes can easily infiltrate into the coating interior and reside there for extended periods. This long-term retention induces lattice distortion, structural damage, and hydrogen embrittlement, ultimately resulting in coating failure [11,12]. However, systematic studies regarding the deuterium and tritium aging behaviors of HBCs remain scarce, and their long-term service stability has yet to be fully elucidated.

Herein, α-Al_2O_3 composite coatings were fabricated via a thermochemical reaction method. Their resistance to Li_4SiO_4 solid breeder corrosion and deuterium aging behaviors were systematically investigated. Microstructural and phase analyses, combined with barrier performance evaluations, revealed the degradation mechanisms under simulated service conditions. Critically, the coatings exhibited excellent corrosion stability, maintaining a permeation reduction factor (PRF) up to two orders of magnitude at 400–500 °C after 16 days of corrosion. Furthermore, after 6 months of long-term aging under a 50 kPa pure D_2 atmosphere, the coatings showed negligible changes in phase and morphology, preserving a dense structure with strong substrate adhesion and a high-temperature PRF of three orders of magnitude.

Our previous work established the fundamental fabrication methodology of the α-Al_2O_3 composite coating and elucidated its mechanical toughening and pristine deuterium barrier mechanisms tailored by in situ grown $AlPO_4$ nanosheets [13]. However, the structural evolution, chemical compatibility, and barrier sustainability of this coating system in the service environment remain entirely unexplored. To bridge this critical knowledge gap, in this work, we systematically investigated the long-term service reliability and chemical stability of this composite coating under both extended isotope exposure and severe chemical corrosion. The results yield critical insights into designing highly reliable HBCs and understanding their performance evolution under harsh fusion environments.

2. Materials and Methods

2.1. Materials

Polished 321 stainless steel (Cr 18%, Ni 10%, Mn 2%, Si 1%, balanced by Fe) was used as a substrate for coating deposition due to its outstanding thermal stability and chemical resistance. Phosphoric acid (H_3PO_4, 85%), aluminum hydroxide ($Al(OH)_3$), and zinc oxide (ZnO, 98%) were purchased from Sinopharm Chemical Reagent Co., Ltd. (Shanghai, China). Nanosize α-Al_2O_3 powders (30–100 nm, 99.9%) were obtained from Macklin Biochemical Co., Ltd. (Shanghai, China). All chemicals were of analytical grade or higher and used as received without further purification.

2.2. Preparation of the α-Al_2O_3 Composite Coatings

To prepare the composite coatings, commercial 321 stainless steel (φ12 mm × 0.5 mm) was utilized as substrates. Prior to deposition, these substrates underwent grinding with 1200-mesh abrasive papers, followed by sequential cleaning in deionized water and ethanol. Structurally, the preparation involved three consecutive steps. First, to prepare the composite coating, H_3PO_4, $Al(OH)_3$, and deionized water were mixed together with a molar ratio of H_3PO_4 to $Al(OH)_3$ of 1:1, and the mixture was stirred until it became clear. Secondly, ZnO and a moderate quantity of H_3PO_4 were introduced into the blended solution. The

resulting mixture was stabilized under stirring at 80 °C for another 2 h. Thereafter, α-Al_2O_3 powders were introduced into the solution with a weight ratio of 10% under vigorous agitation to form a uniform slurry. Finally, the slurry was dip-coated onto the substrates under ambient conditions, and the coated samples were first baked at 80 °C for 1 h and then annealed in a muffle furnace at 500 °C in air for 2 h with a heating rate of 10 °C/min.

2.3. Characterization and Performance Testing

Surface morphology and microstructure were examined by field-emission scanning electron microscopy (FE-SEM, Zeiss Sigma 300, Carl Zeiss AG, Oberkochen, Germany). The crystalline phases of the α-Al_2O_3 composite coatings were identified by X-ray diffraction (XRD, Bruker D8 Advance, Bruker AXS GmbH, Karlsruhe, Germany) using a Cu Kα radiation source (λ = 1.5418 Å) at a scanning rate of 5°/min. X-ray photoelectron spectroscopy (XPS, AXIS-ULTRA DLD-600W, Shimadzu-Kratos, Shimadzu Corporation, Kyoto, Japan) was employed to probe surface chemical states and defect-related features.

2.4. Li_4SiO_4 Corrosion Resistance Test

The chemical compatibility of the coatings was evaluated using a static solid-state corrosion method. The steel with coating was completely embedded in solid Li_4SiO_4 ceramic powder inside a high-temperature-resistant crucible to ensure uniform surface contact. The crucible was subsequently placed in a tube furnace and subjected to isothermal heat treatment under a He/H_2 (99 vol.% He and 1 vol.% H_2) mixed atmosphere, simulating the purge gas environment of a fusion reactor blanket. The corrosion temperature was maintained at 550 °C, with isothermal exposure times set to 2, 8, and 16 days.

2.5. Hydrogen Isotope Aging Test

Static deuterium aging experiments were conducted in a custom 1000 mL stainless-steel pressure vessel to evaluate the long-term hydrogen isotope exposure behavior of the α-Al_2O_3/(Al-Zn)PO_4 composite coatings. Prior to exposure, the steel with coating was loaded into the vessel, which was then evacuated to a high vacuum level. Pure deuterium gas (D_2) was subsequently introduced into the vessel, and the charging pressure was precisely maintained at 50 kPa. The sealed vessel was kept under ambient laboratory conditions for a long-term storage period of 6 months.

2.6. Hydrogen Permeation Resistance Measurement

Deuterium was selected as a surrogate for tritium to avoid radioactivity and minimize atmospheric hydrogen interference. To investigate the impact of corrosion and aging on the barrier performance of the coatings, gas-driven permeation tests were performed on the following specimens: pristine uncoated 321 stainless steel (serving as the unified baseline reference), the steel with pristine coating, the steel with coatings after corrosion for 2, 8, and 16 days, and the steel with coating after 6 months of aging. Permeation measurements were performed using a gas-driven permeation system detailed in ref. [14], where the specimen was sealed between the upstream and downstream chambers. Prior to testing, both chambers were evacuated to a high vacuum level (10^{-5} Pa). Deuterium gas was then introduced into the upstream chamber and stabilized at 40 kPa. Driven by the resulting pressure gradient, deuterium permeated through the coating/substrate composite into the downstream chamber, where the permeation flux was continuously monitored. Before the permeation test, to ensure the accuracy and reliability of the gas permeation device, we tested the deuterium permeability of the 321 steel substrate and compared the obtained data with the reported values of the same material in the studies, finding that the permeability of 321 steel from our device agreed well with those reported previously [15]. During the test, the exposed area of the specimen was about 10 mm, and

the permeation flux was continuously monitored until a rigorous steady-state was achieved, defined as a signal fluctuation of less than 5% for over 60 min. All measurements were conducted within 400–500 °C to simulate the typical operating temperatures of tritium barriers in fusion reactors. The deuterium permeability was calculated according to ref. [16]. The permeation rate of hydrogen isotopes is quantitatively described by the flux J under steady-state conditions:

$$J = \frac{P \cdot p^n}{d} \quad (1)$$

$$P = \frac{J \cdot d}{p^n} \quad (2)$$

where J is the hydrogen permeation flux (mol $m^{-2} \cdot s^{-1}$); P is the permeability (mol $m^{-1} \cdot s^{-1} \cdot Pa^{-n}$); p is the upstream gas pressure (Pa); d is the sample thickness (m); and n reflects the hydrogen diffusion model. Generally, the deuterium transport in the coatings is predominantly governed by a bulk-diffusion-controlled mechanism; in this case, n = 0.5 was adopted [16]. To guarantee the reproducibility and statistical reliability of the transport kinetics, all gas-phase deuterium permeation measurements across the entire temperature range were performed on three independent parallel specimens for each state. The permeability data points presented in this work represent the mean values of these independent runs.

3. Results and Discussion

3.1. Corrosion Behavior of the α-Al_2O_3 Composite Coatings

As demonstrated in our previous work [13], the fabrication of the α-Al_2O_3 coatings reinforced by in situ grown $AlPO_4$ nanosheets involves a chemical slurry deposition approach combined with subsequent heat treatment. α-Al_2O_3 nanoparticles were incorporated into the (Al-Zn)H_2PO_4 precursor solution, functioning as heterogeneous nucleation templates that guide the crystallization of $Al(H_2PO_4)_3$ and drive the in situ formation of $AlPO_4$ nanosheets during the subsequent thermal treatment. Upon annealing at 500 °C, the $Al(H_2PO_4)_3$ precursor decomposed and transformed into crystalline $AlPO_4$, whereas $Zn(H_2PO_4)_2$ was converted into $Zn_3(PO_4)_2$ and $Zn_2P_2O_7$. These concurrent phase transitions ultimately yielded a chemically stable α-Al_2O_3/(Al-Zn)PO_4 composite architecture. The detailed information regarding the morphology and composition of the as-synthesized coatings can be found in the previous work [13], and all comparisons presented in the current study are related to these previous results.

Li_4SiO_4 tritium breeders are widely applied in nuclear fusion blankets and directly contact hydrogen barrier coatings. Therefore, chemical compatibility with Li_4SiO_4 is a crucial indicator for HBC evaluation [17,18]. Importantly, a comparison with previously reported hydrogen permeation barrier coatings, as displayed in our previous work [13], has confirmed the superior hydrogen barrier efficiency of this α-Al_2O_3 composite coating, thereby inspiring us to further explore its long-term anti-corrosion performance under extreme conditions. Here, α-Al_2O_3 composite coatings were packed with solid Li_4SiO_4 powders and annealed at 550 °C for 2, 8, and 16 days to study the structural and performance variations during the interaction. Figure 1 shows the surface morphologies after corrosion for different durations. Figure 1a,d display the SEM images of the 2-day corroded sample at different magnifications. Compared to the pristine coating, a certain number of small particles attached to the surface, and fine fish-scale-like structures emerged, indicating that the coating reacted with Li_4SiO_4 within 2 days at 550 °C. As the corrosion time increased, the granular substances proliferated and the scaly structures became denser, which also induced microcracks on the surface due to the degradation of the original coating structure. Additionally, the high-temperature thermal decomposition of the Li_4SiO_4

powder produced small particulates that adhered to the surface. Figure 1g,h present the surface EDS mappings after 2 and 8 days of corrosion, revealing that the elements are still uniformly distributed and dense. This confirms that the intrinsic structure of the α-Al_2O_3 composite coating was not fatally damaged, retaining its integrity.

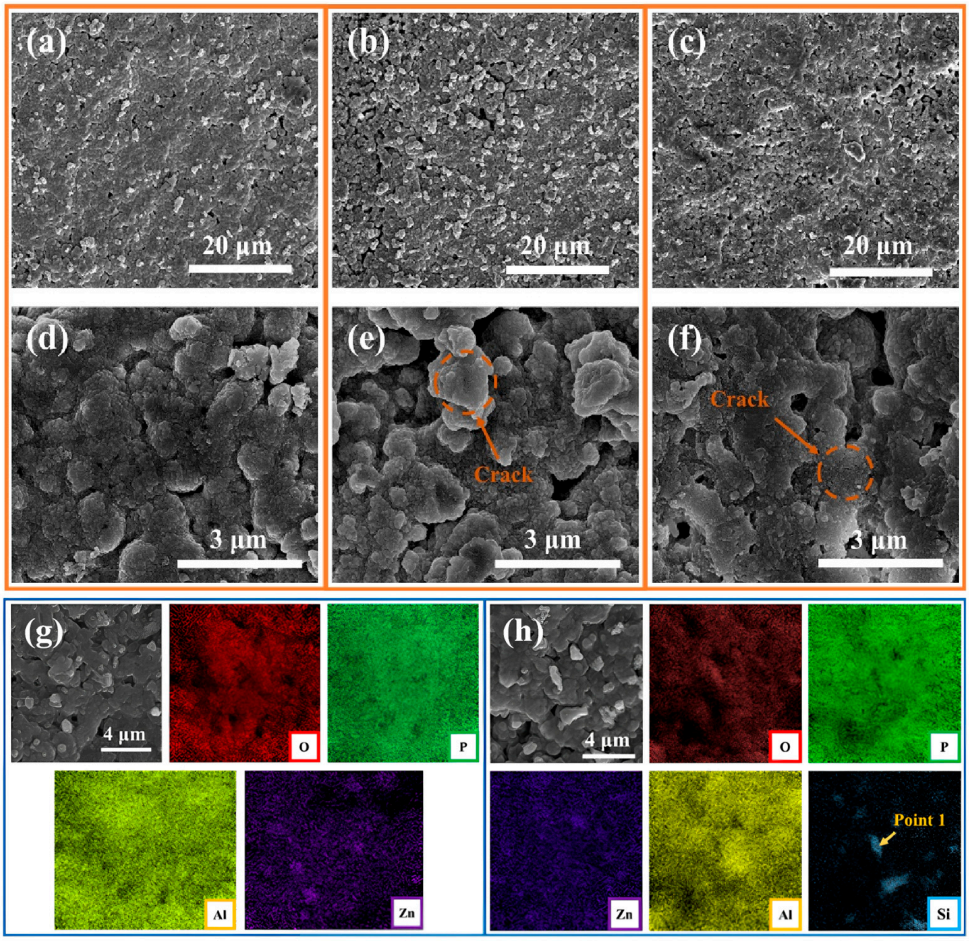


Figure 1. SEM micrographs and EDS mappings of the α-Al_2O_3/(Al-Zn)PO_4 composite coatings after corrosion with Li_4SiO_4 powders for varying durations: SEM images for (**a**,**d**) 2 days, (**b**,**e**) 8 days, and (**c**,**f**) 16 days; EDS elemental mappings for (**g**) 2 days and (**h**) 8 days.

The surface elemental atomic percentages after different corrosion times are summarized in Table 1. As summarized in Table 1, an obviously localized Si enrichment was detected within these specific micro-domains after prolonged exposure. It was noticed that, in the 2-day corroded sample, the Si concentration was almost negligible and remained well below the detection limit of the EDS instrument. This noticeable accumulation implies a progressive inward diffusion of Si from the Li_4SiO_4 over time.

Table 1. Elemental atomic percentages of the coatings after corrosion for varying durations.

Atomic Percent	Zn	Al	O	P	Si
2-day EDS mapping	4.39	16.68	63.34	14.51	-
8-day EDS mapping	14.59	14.06	58.07	12.70	0.61
8-day EDS point	14.10	13.95	58.96	12.05	0.93

To investigate the internal corrosion propagation within the coatings, cross-sectional EDS elemental mappings of the samples after 2 and 8 days of exposure were performed, as illustrated in Figure 2. The cross-sections initially present a relatively dense architecture

with homogeneous elemental distributions; however, distinct micropores and microcracks become observable within the coating interior after 8 days of isothermal holding. This structural degradation implies a coefficient of thermal expansion mismatch between the Li_4SiO_4 reaction products and the pristine coating matrix, which induces thermal stresses and subsequent crack initiation during the thermal cycling, thereby compromising the structural compactness. Furthermore, the cross-sectional EDS profiles reveal the presence of a traceable amount of Si within the coating interior, where no detectable Si diffusion was noticed after 2 days of corrosion, whereas a distinct forward diffusion of Si into the coating matrix could be observed when the corrosion time was extended to 8 days, with the local Si content increasing from 0% to 0.61%. It is inferred that the Si species originating from the thermal decomposition products diffused into the coating matrix under the long-term corrosion environment, which inevitably detriments the barrier performance of the composite coating to some extent.

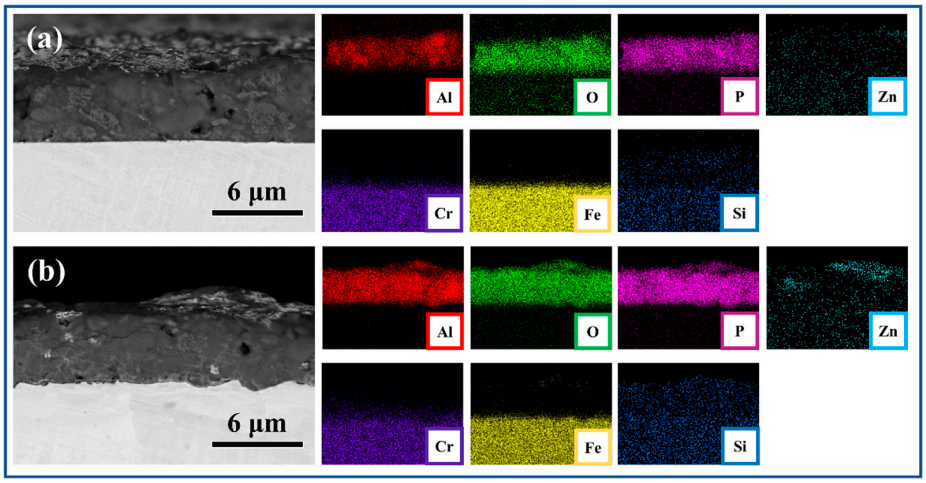


Figure 2. Cross-sectional SEM images and EDS mappings of the α-Al_2O_3/(Al-Zn)PO_4 composite coatings corroded by Li_4SiO_4 powders for (**a**) 2 days and (**b**) 8 days.

The XRD patterns of the coatings after corrosion with Li_4SiO_4 powders for different durations are shown in Figure 3. Phase analysis reveals that in addition to the original components, $LiZn(PO_4)$ and $Li_4(P_2O_7)$ were generated on the coating surface. This indicates that the decomposed Li_4SiO_4 reacted with the surface phosphates under high temperatures, forming these lithium-containing compounds. As the contact time increased, no new substances appeared, and the diffraction peaks of $LiZn(PO_4)$ and $Li_4(P_2O_7)$ showed no significant changes. This suggests that the reaction between Li_4SiO_4 and the α-Al_2O_3/(Al-Zn)PO_4 composite coating becomes sluggish after 2 days and tends to stabilize.

To further scrutinize the phase composition of the corrosion products on the coating surface, high-resolution X-ray photoelectron spectroscopy (XPS) was conducted, as illustrated in Figure 4. The XPS survey and core-level spectra not only detect the intrinsic Al, Zn, P, and O elements from the coating matrix, but also identify the presence of Li and Si species originating from the Li_4SiO_4 breeder [19]. This elemental intrusion directly demonstrates that a chemical reaction occurred between Li_4SiO_4 (or its thermal decomposition products) and the composite coating, which is in good agreement with the aforementioned XRD findings. Characteristically, the pristine matrix peaks, such as Al 2p at 74.3 eV and lattice oxygen in O 1s at 531.1 eV, exhibit well-defined symmetric profiles with a full width at half maximum (FWHM) of 1.2–1.3 eV. The Li 1s core-level spectrum exhibits a binding energy (BE) peak at 55.8 eV, which is perceptibly higher than that reported for the pristine Li_4SiO_4 phase (~54 eV). This positive BE shift indicates the thermal decomposition of the Li_4SiO_4 powder into Li_2O (55.5 eV) and its subsequent interaction with the coating constituents to

precipitate $LiZn(PO_4)$ and $Li_4(P_2O_7)$ [20]. In the O 1s spectrum, the peak located at 531.7 eV is assigned to the oxygen anions in Li_4SiO_4, whereas the other component peaks remain identical to those of the pristine coating before corrosion. Regarding the Si 2p spectrum, the peak at 101.9 eV corresponds to the Si state in Li_4SiO_4. As spin–orbit splitting is generally negligible for silicon complexes, a singlet fitting protocol was adopted for this chemical state. Additionally, an auxiliary Si peak detected at 102.8 eV is presumably attributed to the silicate-based decomposition derivatives of Li_4SiO_4 [21].

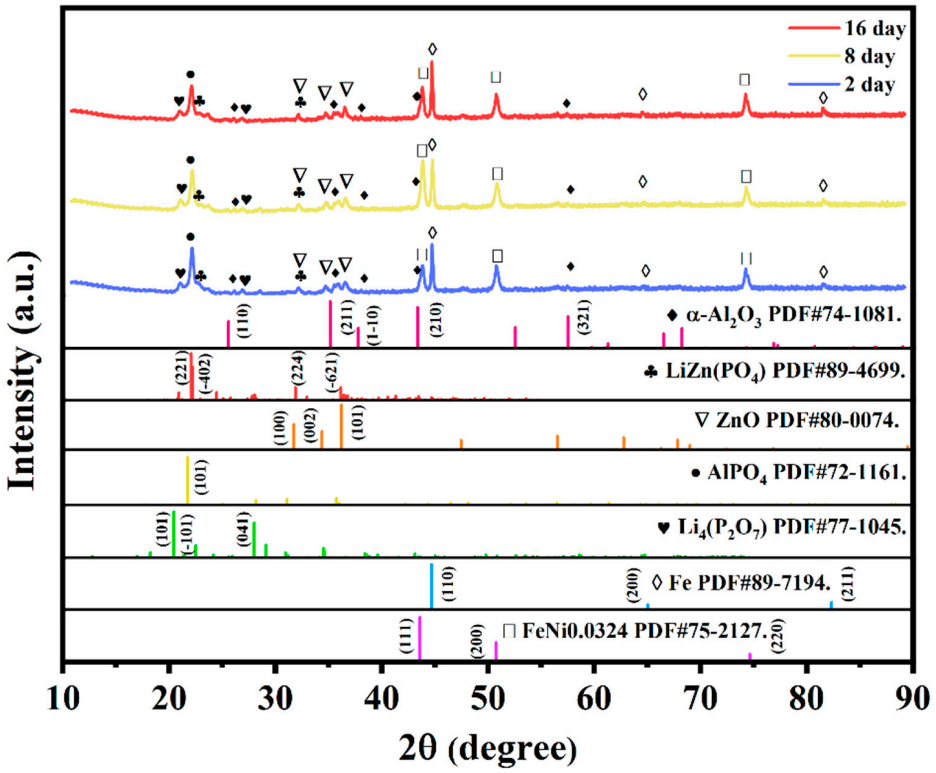


Figure 3. XRD patterns of the α-Al_2O_3/(Al-Zn)PO_4 composite coatings after corrosion with Li_4SiO_4 powder for varying durations.

3.2. Hydrogen Permeation Resistance of the Coatings After Corrosion

Hydrogen barrier performance of the coatings after different corrosion times was evaluated at 400–500 °C, as shown in Figure 5. Hydrogen barrier performance of the coatings after different corrosion times was evaluated at 400–500 °C, as shown in Figure 5. Figure 5a shows the variation trends of the barrier performance under different testing temperatures, and Figure 5b presents a direct comparison of the barrier performance evolution after different corrosion times. It is worth noting that, owing to the radioactivity of tritium, deuterium was used instead for the permeation tests in this study. For the 2-day corroded sample, the deuterium permeability at 500 °C is significantly suppressed, exhibiting a reduction of 847 times compared to that of the bare 321 stainless-steel substrate. With the corrosion time extended to 8 days, the permeability reduction factor at 500 °C decreases to 220 times relative to the 321 substrate. Even after 16 days of severe corrosion, the reduction in permeability over the entire testing temperature range still remains above two orders of magnitude (>10^2 times), demonstrating excellent resistance to Li_4SiO_4 corrosion. Interestingly, the PRF decrease at a lower temperature of 400 °C is smaller, and even a slight increase is observed after 2 days, indicating that the coating maintains stable or even locally enhanced barrier capabilities under mild corrosion. Even after 16 days of severe corrosion, the coating still acts as an effective hydrogen barrier, reflecting high structural stability and durability. Firstly, the thermal expansion mismatch between the reaction

products and the coating generates thermal cracks at high temperatures, decreasing coating density. Cross-sectional SEM images also confirm that distinct crack propagation channels were formed inside the coating after 8 days of corrosion, thereby accelerating deuterium permeation. However, as the corrosion time increased, the secondary pyrolysis products derived from Li_4SiO_4 powder formed micro-sized particles that continuously adhered to the coating surface. These granular products effectively migrated into and clogged the thermal-stress-induced micro-cracks, successfully providing a physical self-healing effect that obstructed the interconnected pathways for hydrogen isotope transport. This self-healing mechanism is further substantiated by the XRD results, which explicitly confirm the presence of these crystalline pyrolysis phases on the surface. Consequently, the combination of physical degradation and dynamic self-healing drives the overall hydrogen resistance toward a stable plateau rather than a continuous sharp drop. Overall, the performance decay exhibits a logarithmic deceleration character.

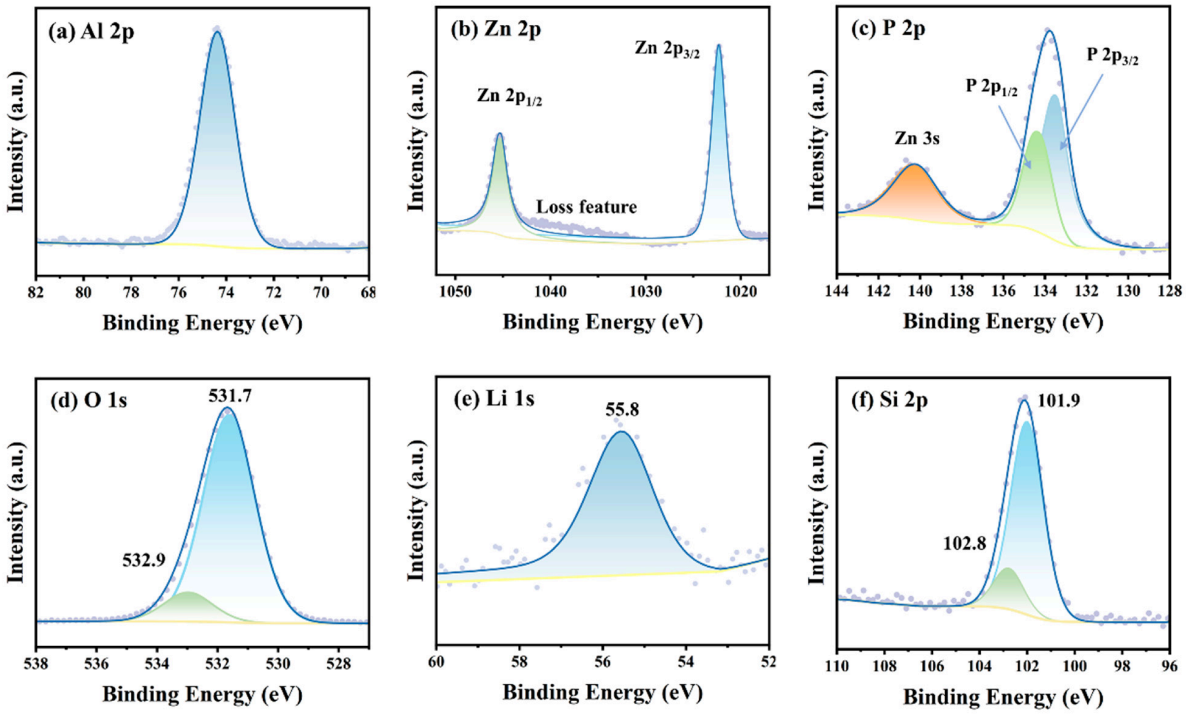


Figure 4. XPS spectra of the α-Al_2O_3/(Al-Zn)PO_4 composite coating after 8 days of corrosion with Li_4SiO_4 powders: (**a**) Al 2p; (**b**) Zn 2p; (**c**) P 2p; (**d**) O 1s; (**e**) Li 1s; (**f**) Si 2p.

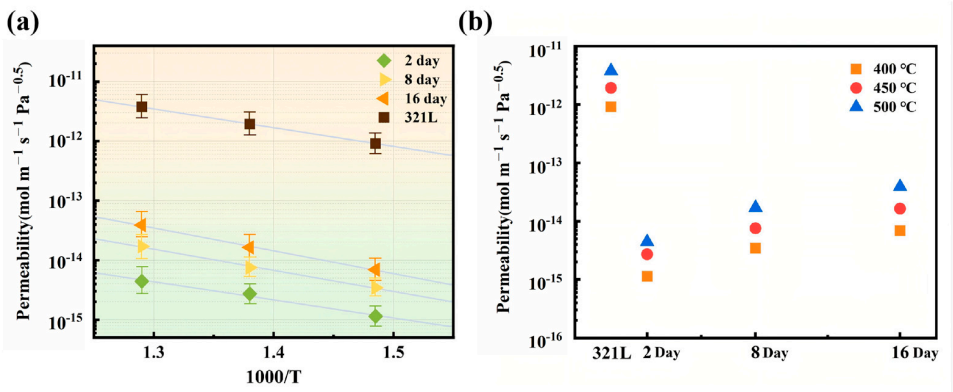


Figure 5. Deuterium permeability of the α-Al_2O_3/(Al-Zn)PO_4 composite coatings after corrosion with Li_4SiO_4 powders for varying durations: (**a**) as a function of testing temperature, and (**b**) as a function of corrosion duration.

3.3. Deuterium Aging Behavior of the α-Al_2O_3 Composite Coatings

Hydrogen permeation barrier coatings (HBCs) applied in nuclear fusion reactors inevitably confront harsh and complex service conditions. The pervasive presence of immense amounts of deuterium (D) and tritium (T) isotopes within the reactor blankets induces prolonged material aging during long-term service [22,23]. Due to their minute atomic radii, these hydrogen isotopes can effortlessly infiltrate into the structural materials and reside therein for extended periods, subsequently destroying the baseline structural configurations and triggering devastating issues such as hydrogen embrittlement and catastrophic failure [9]. Consequently, maintaining a robust hydrogen permeation resistance against long-term deuterium/tritium-induced aging is a paramount prerequisite for HBCs. To thoroughly evaluate this capability, the α-Al_2O_3 composite coatings fabricated via the thermochemical reaction method were enclosed within sealed stainless-steel canisters under a 50 kPa pure D_2 atmosphere to systematically explore their long-term deuterium aging performance.

Figure 6 illustrates the grazing incidence X-ray diffraction (GIXRD) patterns of the α-Al_2O_3/(Al-Zn)PO_4 composite coatings before and after the 6-month deuterium aging experiment. Phase evolution analysis reveals that the surface chemical constituents of the composite coating remain virtually invariant even after a 6-month exposure to the 50 kPa D_2 environment. Owing to the surface-sensitive nature of the GIXRD configuration, the diffraction reflections corresponding to the underlying steel substrate appear relatively weak. Notably, the diffraction peaks belonging to $AlPO_4$ exhibit none of the structural shifts typically observed in conventional α-Al_2O_3 composite coatings. This enhanced stability is ascribed to the fact that the $AlPO_4$ phase within the current α-Al_2O_3/(Al-Zn)PO_4 system predominantly crystallizes into a highly stable, cristobalite-type $AlPO_4$ modification. These stable phases are morphologically distributed throughout the matrix as distinct nanosheets, which are remarkably immune to phase transformations potentially induced by the surface-adsorbed deuterium species. Consequently, the GIXRD analysis firmly corroborates that the α-Al_2O_3/(Al-Zn)PO_4 composite coating possesses exceptional phase stability within deuterium-charged service environments.

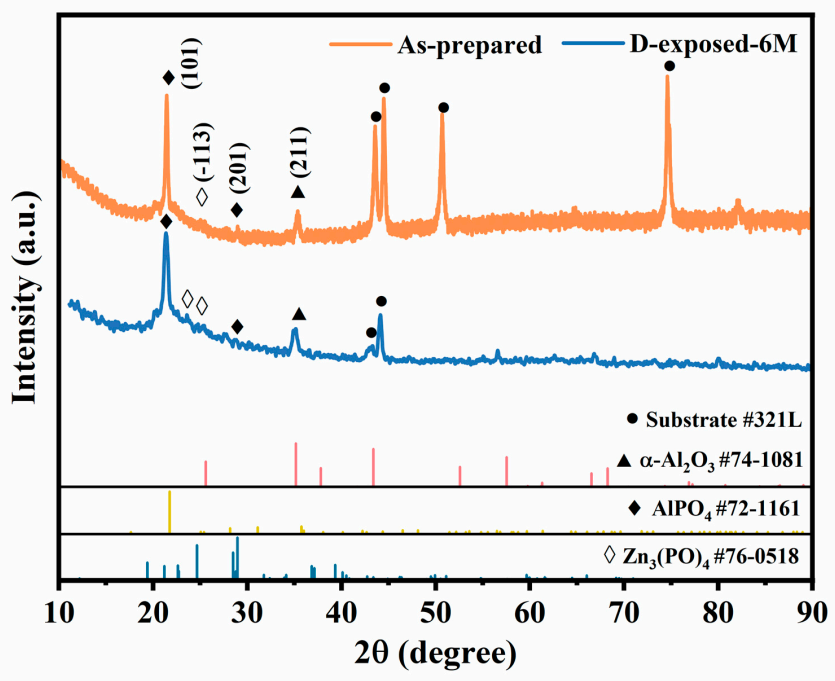


Figure 6. XRD patterns of the α-Al_2O_3/(Al-Zn)PO_4 composite coatings after the 6-month deuterium aging experiment.

Figure 7 displays the surface and cross-sectional SEM micrographs of the α-Al_2O_3 composite coating after the 6-month deuterium aging experiment. The coating surface remains highly homogeneous and dense, with no discernible pores or microcracks. The intrinsic $AlPO_4$ nanosheets within the coating are distinctly observable, exhibiting negligible morphological deviation compared to their pristine state before aging. Cross-sectional views reveal that the coating is devoid of macrocracks or through-thickness penetrating defects, although a few isolated micropores are present. Furthermore, a robust interfacial adhesion between the coating and the substrate is preserved. This superior bonding status is attributed to the high interfacial strength and enhanced toughness inherent to the α-Al_2O_3 composite system, which successfully prevents delamination from the substrate during the long-term aging process. Figure 8 depicts the surface EDS elemental mappings of the composite coating post deuterium exposure. The spatial distributions of Al and Zn elements exhibit localized non-uniformity, which is consistent with the morphology of the $AlPO_4$ phase residing as discrete nanosheets. Interestingly, several localized aggregations of the Fe signal are detectable. It is inferred that minute micropores or localized thinning occurred at these specific sites during the experiment; the limited local thickness of the coating consequently allowed the primary electron beam to penetrate through the matrix and excite the characteristic Fe signal from the underlying steel substrate.

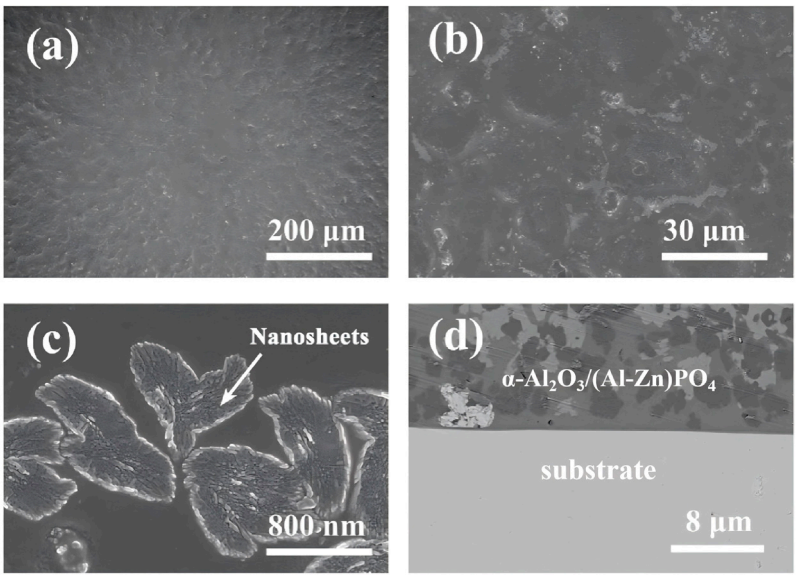


Figure 7. SEM micrographs of the α-Al_2O_3/(Al-Zn)PO_4 composite coatings after the 6-month deuterium aging experiment: (**a**–**c**) surface images; (**d**) cross-sectional image.

Figure 9 presents the high-resolution XPS core-level spectra of Al 2p, Zn 2p, P 2p, and O 1s for the α-Al_2O_3/(Al-Zn)PO_4 composite coating after the 6-month deuterium aging experiment. This analysis aims to verify whether the chemical bonding configurations of the pristine coating are altered during the long-term exposure. Compared with the baseline profiles before aging, the binding energies (BEs) of each characteristic peak exhibit no discernible shifts. This invariance firmly demonstrates that the composite coating remained chemically inert toward deuterium. It did not form any deuterium-bearing chemical bonds during service, thereby validating its exceptional deuterium aging resistance. Specifically, the auxiliary peak located at 140.1 eV within the P 2p spectrum is assigned to the Zn 3s photoemission [24–26]. Meanwhile, the emergence of the peak at 533.7 eV in the O 1s spectrum is presumably correlated with adventitious surface contamination or the adsorption of ambient oxygen species.

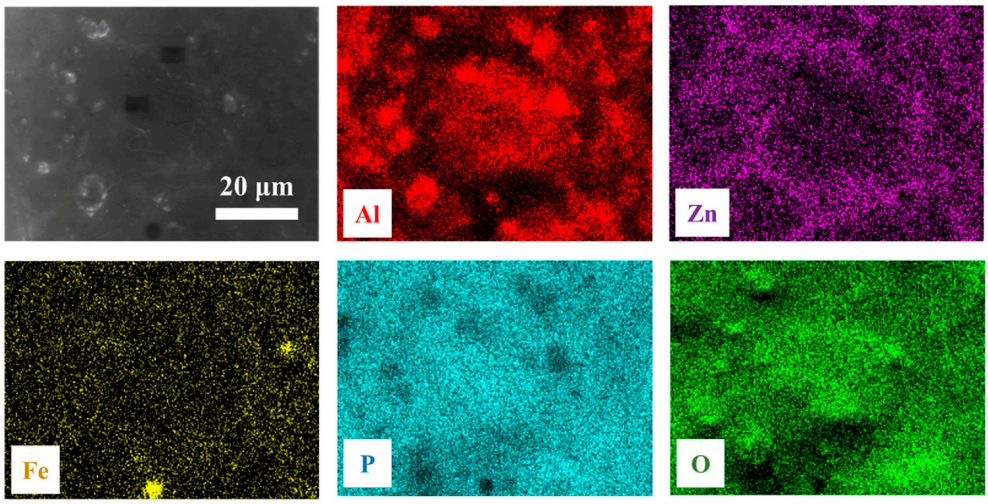


Figure 8. Surface EDS elemental mapping of the α-Al_2O_3/(Al-Zn)PO_4 composite coating after the 6-month deuterium aging experiment.

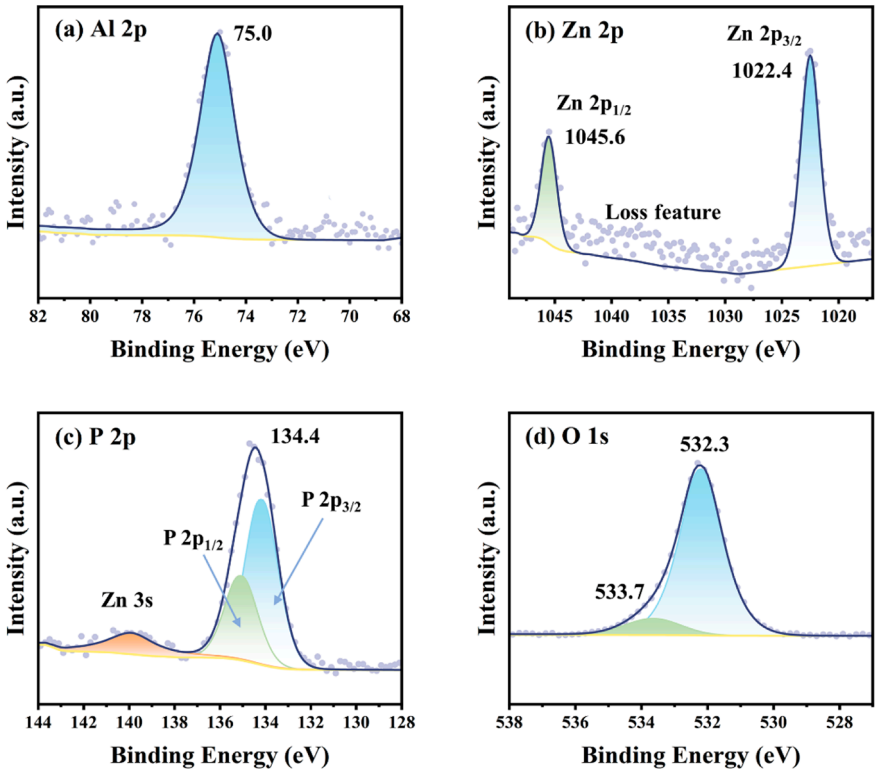


Figure 9. XPS spectra of the α-Al_2O_3/(Al-Zn)PO_4 composite coating after the 6-month deuterium aging experiment: (**a**) Al 2p; (**b**) Zn 2p; (**c**) P 2p; (**d**) O 1s.

3.4. Hydrogen Permeation Resistance of the Coatings After Deuterium Aging

Figure 10 displays the deuterium permeability of the α-Al_2O_3 composite coating after the 6-month aging experiment. As shown in Figure 10a, the deuterium permeability of the aged coating follows a linear Arrhenius relationship with respect to the reciprocal temperature (1/T). Crucially, it reveals that the composite coating still exhibits a remarkable deuterium barrier capability compared to the bare substrate [20]. At 500 °C, the permeability decreases by at least three orders of magnitude, reaching a low value of 2.59×10^{-15} mol m^{-1} s^{-1} $Pa^{-1/2}$, which represents a reduction of 1452 times relative to the substrate. Within the testing temperature range of 400–500 °C, the permeability reduction remains highly effective, exhibiting a decrease of 669 to 1452 times compared to the substrate. Compared

to the pristine coating at the same temperatures, the lower deuterium permeability in the aged samples is speculated to result from the introduction of deuterium atoms into the coating during the aging process. The existence of deuterium atoms inside the coating before the permeation test may help to inhibit the subsequent deuterium diffusion in the coating. These results confirm that the coating maintains an excellent deuterium barrier performance even after long-term deuterium exposure.

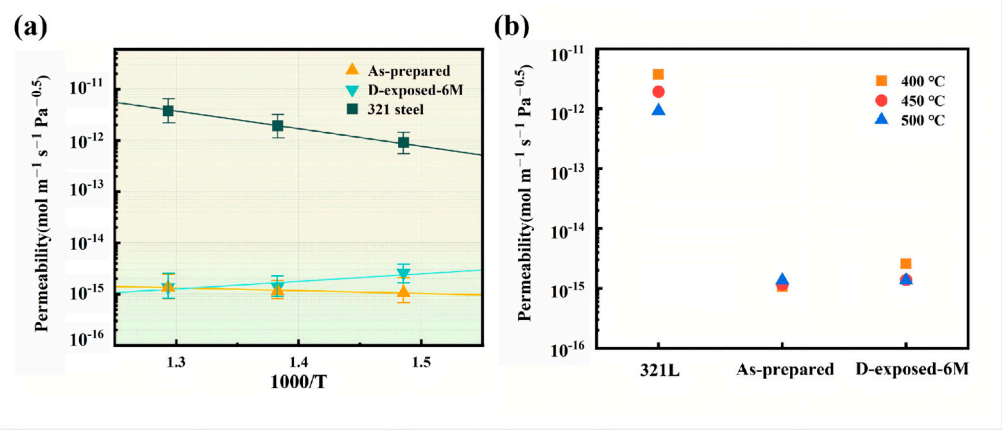


Figure 10. Deuterium permeability of the α-Al_2O_3/(Al-Zn)PO_4 composite coatings after a 6-month deuterium aging experiment: (**a**) as a function of testing temperature, and (**b**) comparison before and after deuterium aging.

This remarkable performance after long-term deuterium aging is primarily sustained by the in situ formed $AlPO_4$ nanosheet architecture [27–29], which effectively enhances both the mechanical integrity and the barrier properties of the coating. Consequently, it suppresses the nucleation of microcracks and through-thickness penetrating defects under prolonged deuterium exposure. The coating thus preserves high structural integrity and robust barrier reliability. Overall, these findings provide a vital experimental foundation for evaluating the service reliability of composite hydrogen barrier coatings in extreme fusion environments.

4. Conclusions

In summary, the Li_4SiO_4 corrosion resistance and deuterium aging behavior of the α-Al_2O_3 composite hydrogen barrier coating (HBC) were systematically investigated under simulated fusion conditions. The main conclusions are summarized as follows:

(1) Corrosion Resistance: The coating exhibits good chemical compatibility with the Li_4SiO_4 tritium breeder, remaining dense and defect-free after 2 days of corrosion at 550 °C in He/H_2.

(2) Durable Barrier Performance: Despite 16 days of severe corrosion, the coating maintains a permeability reduction of over two orders of magnitude (>10^2 times) relative to the bare steel substrate, confirming its stable corrosion resistance.

(3) Long-term Aging Stability: After a 6-month deuterium aging experiment, the coating retains its dense microstructure, crack-free matrix, and strong substrate adhesion, while preserving a 1452-fold reduction in permeability at 500 °C.

Overall, the α-Al_2O_3 composite coating demonstrates outstanding structural stability and barrier reliability under simulated fusion conditions. This work systematically reveals the intrinsic correlation between structural evolution and performance degradation. Ultimately, these findings provide a vital experimental foundation and an innovative design strategy for understanding the hydrogen isotope permeation behavior of composite barrier

coatings under complex service conditions. Considering that the long-term degradation kinetics were evaluated under static conditions, further studies are still needed in the future, with the effects of neutron irradiation, thermal cycling, and plasma exposure taken into consideration, given the multi-field coupling environments in fusion reactors.

Author Contributions: H.Y.: Investigation, Formal analysis, Writing—original draft. S.L.: Formal analysis, Writing—original draft. X.W.: Supervision, Resources. H.L.: Supervision, Conceptualization, Writing—review & editing, Funding acquisition. All authors have read and agreed to the published version of the manuscript.

Funding: This work was funded by the National Key Research and Development Program of China (Grant No. 2023YFB3508600), the National Natural Science Foundation of China (Grant Nos. 52553007 and 52273224), and the Guangdong Basic and Applied Basic Research Foundation (Grant No. 2024B1515020045).

Data Availability Statement: Dataset available on request from the authors.

Conflicts of Interest: The authors declare no conflicts of interest.

References

1. Vogt, E.T.C.; Weckhuysen, B.M. The Refinery of the Future. *Nature* **2024**, *629*, 295–306. [CrossRef] [PubMed]
2. Liu, F.; Yu, H.; Yi, X.; Deng, S.; Li, S.; Yabuuchi, K.; Ohnuki, S. Microstructure Evolution of γ-Al_2O_3/FeAl Tritium Permeation Barrier Coatings Under 6.4 MeV Fe^{3+} Ion Irradiation. *Nucl. Mater. Energy* **2024**, *38*, 101627. [CrossRef]
3. Chikada, T.; Fujita, H.; Tokitani, M.; Hishinuma, Y.; Terai, T.; Oya, Y. Deuterium Permeation through Monoclinic Erbium Oxide Coating. *Fusion Eng. Des.* **2018**, *133*, 121–124. [CrossRef]
4. Xiang, X.; Yang, F.; Zhang, G.; Wang, X. Effect of Steel Substrates on the Formation and Deuterium Permeation Resistance of Aluminide Coatings. *Coatings* **2019**, *9*, 95. [CrossRef]
5. Akahoshi, E.; Matsunaga, M.; Kimura, K.; Nakamura, K.; Saito, K.; Hishinuma, Y.; Tanaka, T.; Chikada, T. Deuterium Permeation through Multi-Layer Ceramic Coatings Under Liquid Lithium-Lead Exposure Condition. *Corros. Sci.* **2021**, *189*, 109583. [CrossRef]
6. Li, Q.; Wang, J.; Xiang, Q.; Yan, K.; Tang, T.; Rao, Y.; Cao, J. Novel Nano-Crystalline Er_2O_3 Hydrogen Isotopes Permeation Barriers. *J. Eur. Ceram. Soc.* **2017**, *37*, 249–254. [CrossRef]
7. Cheng, H.; Luo, H.; Li, Y.; Rao, Z.; Zhao, Q.; Pan, Z.; Kong, Q.; Li, X.; Raabe, D. Segregation Passivation Makes Cost-Effective Stainless Steel Resistant to Corrosion and Hydrogen Embrittlement. *Sci. Adv.* **2026**, *12*, eadz1833. [CrossRef] [PubMed]
8. Nemanič, V. Hydrogen Permeation Barriers: Basic Requirements, Materials Selection, Deposition Methods, and Quality Evaluation. *Nucl. Mater. Energy* **2019**, *19*, 451–457. [CrossRef]
9. Zhu, C.; Zhang, W.; Wang, L. Effect of Thermal Cycles on Structure and Deuterium Permeation of Al_2O_3 Coating Prepared by MOD Method. *Fusion Eng. Des.* **2020**, *159*, 111750. [CrossRef]
10. Endoh, R.; Nogami, S.; Hishinuma, Y.; Chikada, T. Submicron-Thick Yttria-Stabilized Zirconia Coating as an Advanced Tritium Permeation Barrier. *Nucl. Fusion* **2021**, *61*, 76015. [CrossRef]
11. Xiao, S.; Meng, X.; Shi, K.; Liu, L.; Wu, H.; Lian, W.; Zhou, C.; Lyu, Y.; Chu, P.K. Hydrogen Permeation Barriers and Preparation Techniques: A Review. *J. Vac. Sci. Technol. A* **2022**, *40*, 060803. [CrossRef]
12. Marques, S.C.; Castilho, A.V.; Dos Santos, D.S. Effect of Alloying Elements on the Hydrogen Diffusion and Trapping in High Entropy Alloys. *Scr. Mater.* **2021**, *201*, 113957. [CrossRef]
13. Li, H.; Liu, S.; Zheng, Z.; Fan, G.; Yan, Y.; Wang, X. One-Step Fabrication of $AlPO_4$ Nanosheet Reinforced Ceramic Coatings with Improved Fracture Toughness and Hydrogen Resistance. *J. Mater. Process. Technol.* **2024**, *333*, 118597. [CrossRef]
14. Zheng, L.; Zheng, Z.; Yan, Y.; Wang, X.; Li, H. High Hydrogen Permeation Resistance Achieved in a Novel (AlCrZr)O Ternary Oxide Nanofilm. *J. Adv. Ceram.* **2025**, *14*, 9221064. [CrossRef]
15. Cao, W.; Ge, S.; Song, J.; Chen, C.; Luo, D. A Deuterium Permeation Barrier by Hot Dipping Aluminizing on AISI321 Steel. *Int. J. Hydrogen Energy* **2016**, *41*, 23125–23131. [CrossRef]
16. Yang, H.; Gong, S.; Mo, S. A Novel Ultrathin Nanocrystalline CeO_2 Coating Achieving High Hydrogen Permeation Barrier Performance. *J. Adv. Ceram.* **2026**. [CrossRef]
17. Liu, Y.; Bian, D.; Zhao, Y. The Influence of Curing Agents on Thermal Property and Corrosion Resistance of Chemically Bonded Phosphate Ceramic Coatings. *J. Sol-Gel Sci. Technol.* **2019**, *89*, 403–415. [CrossRef]
18. Kulikov, V.; Kubich, V.; Fasol, Y.; Cherneta, O.; Kvon, S.; Issagulov, A.; Arinova, S.; Zharkevich, O. Modeling Wear of KNA-82 Coatings with 0.5% Yttrium for Radial Seals of Gas Turbine Engines. *Coatings* **2026**, *16*, 261. [CrossRef]

19. Pacanowski, S.; Wachowiak, M.; Jablonski, B.; Szymanski, B.; Smardz, L. Interface Mixing and Hydrogen Absorption in Pd/Mg and Pd/Al/Mg Thin Films. *Int. J. Hydrogen Energy* **2021**, *46*, 806–813. [CrossRef]
20. Yang, H.; Shao, Z.; Wang, W.; Ji, X.; Li, C. A Composite Coating of GO-Al_2O_3 for Tritium Permeation Barrier. *Fusion Eng. Des.* **2020**, *156*, 111689. [CrossRef]
21. Ravizz, E.; Spadoni, S.; Piagge, R.; Comite, P.; Wiemer, C. XPS Composition Study of Stacked Si Oxide/Si Nitride/Si Oxide Nano-Layers. *Surf. Interface Anal.* **2012**, *44*, 1209–1213. [CrossRef]
22. Lu, G.; Zhang, G.; Chen, M.; Wang, X. Tritium Aging Effects On Hydrogen Permeation through Pd8.5Y0.19Ru Alloy Membrane. *Fusion Eng. Des.* **2011**, *86*, 2220–2222. [CrossRef]
23. Krentz, T.M.; Ronevich, J.A.; Balch, D.K.; San Marchi, C. Tritium Embrittlement of Austenitic Stainless-Steel Tubing at Low Helium Contents. *Fusion Eng. Des.* **2021**, *168*, 112413. [CrossRef]
24. Zheng, H.; An, M.; Lu, J. Surface Characterization of the Zn-Ni-Al_2O_3 Nanocomposite Coating Fabricated Under Ultrasound Condition. *Appl. Surf. Sci.* **2008**, *254*, 1644–1650. [CrossRef]
25. Baird, N.; Losovyj, Y.; Yuzik-Klimova, E.Y.; Kuchkina, N.V.; Shifrina, Z.B.; Pink, M.; Stein, B.D.; Morgan, D.G.; Wang, T.; Rubin, M.A.; et al. Zinc-Containing Magnetic Oxides Stabilized by a Polymer: One Phase or Two? *ACS Appl. Mater. Interfaces* **2016**, *8*, 891–899. [CrossRef] [PubMed]
26. Mu, S.; Li, N.; Li, D.; Xu, L. Corrosion Behavior and Composition Analysis of Chromate Passive Film On Electroless Ni-P Coating. *Appl. Surf. Sci.* **2010**, *256*, 4089–4094. [CrossRef]
27. Su, J.; Liu, Y.; Peng, X.; Sun, G.; Jiang, X. Preparation of α-Al_2O_3 by Low-Temperature Calcining γ-Al_2O_3 with A-Phase Seed in-Situ Obtained by Ball Milling. *Mater. Today Commun.* **2023**, *36*, 106681. [CrossRef]
28. Huang, W.; Huang, P.; Huang, C.; Yen, F.; Huang, C. Characterization of Nano-Sized α-Al_2O_3 Compacts Prepared Via Modified θ-Al_2O_3@PEG Technology. *Ceram. Int.* **2022**, *48*, 15932–15938. [CrossRef]
29. Xu, Q.; Chevalier, J.; Amodeo, J. Atomistic Simulation of α-Al_2O_3 Nanoparticle Plastic Anisotropy Under Compression. *J. Am. Ceram. Soc.* **2023**, *106*, 5986–5999. [CrossRef]

Disclaimer/Publisher's Note: The statements, opinions and data contained in all publications are solely those of the individual author(s) and contributor(s) and not of MDPI and/or the editor(s). MDPI and/or the editor(s) disclaim responsibility for any injury to people or property resulting from any ideas, methods, instructions or products referred to in the content.